Essential Kinesins: Characterization of *Caenorhabditis elegans* KLP-15[†]

Gautier Robin,[‡,§] Salvatore DeBonis,[‡] Aurélie Dornier,[∥] Giovanni Cappello,[∥] Christine Ebel,[‡] Richard H. Wade,*[,‡] Danielle Thierry-Mieg,[⊥] and Frank Kozielski*[,‡]

Institut de Biologie Structurale, UMR 5075 CEA/CNRS/UJF, 41 rue Jules Horowitz, 38027 Grenoble Cedex 01, France, Laboratoire de Physico-Chimie, Institut Curie, UMR 168 CNRS/Institut Curie, 11 rue Pierre et Marie Curie, 75231 Paris Cedex 05, France, and National Center for Biotechnology Information, National Library of Medicine, National Institutes of Health, Building 38A, 8600 Rockville Pike, Bethesda, Maryland 20894

Received August 26, 2004; Revised Manuscript Received February 15, 2005

ABSTRACT: Kinesins form a superfamily of molecular motors involved in cell division and intracellular transport. Twenty kinesins have been found in the *Caenorhabditis elegans* genome, and four of these belong to the kinesin-14 subfamily, i.e., kinesins with C-terminal motor domains. Three of these kinesin-14s, KLP-15, KLP-16, and KLP-17, form a distinct subgroup in which KLP-15 and KLP-16 are more than 90% identical and appear to be related by a relatively recent gene duplication. They are essential for meiotic spindle organization and chromosome segregation, and are mostly expressed in the germline. With 587 amino acids each, they are among the smallest kinesins known. Using bacterially expressed KLP-15 constructs with different length extensions preceding the motor domain, we have determined in vitro the following characteristic properties: ATPase activity, microtubule binding, oligomeric state, microtubule gliding activity, and direction of movement. The constructs exhibit a monomer−dimer equilibrium that depends on the length of the predicted α-helical coiled-coil region preceding the motor domain. The longest construct with the complete coiled-coil domain is a stable dimer, and the shortest construct with only seven amino acids preceding the motor domain is a monomer. In microtubule gliding assays, the monomer is immobile whereas the fully dimeric KLP-15 construct supports gliding at 2.3 μm/min and moves toward microtubule minus ends, like other members of the kinesin-14 subfamily studied to date.

Kinesins form a large superfamily of eukaryotic molecular motors which interact with microtubules and participate in intracellular transport and cell division. They transform chemical energy from ATP hydrolysis into mechanical work, allowing them to move rapidly and in a specific direction along microtubules (*1*). Twenty genes encoding kinesin-like proteins have been identified in the *Caenorhabditis elegans* genome (*2*, *3*), and many of these have mammalian orthologues. The in vivo function of several nematode kinesins has been extensively investigated through observations of loss of function phenotypes induced by mutation or RNA interference (*4*−*12*). Although most kinesins have their ∼320-amino acid motor domain close to their N-terminus, there is an important subfamily with the motor domain near the C-terminus of the polypeptide chain; in the proposed new nomenclature, this subfamily is now called the kinesin-14 family (*13*, *14*). There are four kinesin-14s in *C. elegans*, KLP-3,[1] KLP-15, KLP-16, and KLP-17, with the last three forming a distinct subgroup in proximity to *Drosophila melanogaster* ncd and *Saccharomyces cerevisiae* Kar3 (*14*).

KLP-15 and KLP-16 are practically identical proteins with 587 amino acid residues each [ClustalW alignments (*15*) give 91.1% identical, 4.3% strongly similar, and 2.0% weakly similar amino acids for the full-length proteins]. The complete mRNAs for klp-15 and klp-16 are also strikingly similar. They are 93% identical along their entire length (including the UTRs), implying that they may be related by a relatively recent gene duplication. They are on the same chromosome (chromosome 1), as is usual for gene duplications, and are less than four megabases apart. The positions

[†] This research has been funded by grants from ARC (Association pour la Recherche sur le Cancer, Contracts 4210 and 5917) and the CNRS (Centre National de la Recherche Scientifique). G.R. acknowledges support from the Ministère de l'Education Nationale, de la Recherche et de la Technologie (MENRT), and the Ligue Nationale contre le Cancer.

* To whom correspondence should be addressed. E-mail: Frank.Kozielski@ibs.fr (F.K.) or wade@ibs.fr (R.H.W.). Telephone: 0033-4-3878-4024. Fax: 0033-4-3878-5494.

[‡] UMR 5075 CEA/CNRS/UJF.

[§] Current address: Institute for Molecular Bioscience, University of Queensland, Brisbane, Queensland 4072, Australia.

[∥] UMR 168 CNRS/Institut Curie.

[⊥] National Institutes of Health.

[1] Abbreviations: AMPPCP, adenosine 5′-(β-methylene)triphosphate; β-ME, β-mercaptoethanol; CCD, charge-coupled device; DVCAM, digital video camera; DTT, dithiothreitol; EGTA, ethylene bis(oxyethylenenitrilo)tetraacetic acid; IPTG, isopropyl β-D-thiogalactopyranoside; KLP, kinesin-like protein, the equivalent gene is given in small letters; MT(s), microtubule(s); NA, numerical aperture; Ncd, nonclaret disjunctional; NIH, National Institutes of Health; Ni−NTA, nickel−nitriloacetic acid; PCR, polymerase chain reaction; PEM, PIPES, EGTA, magnesium buffer; PIPES, piperazine-*N*,*N*′-bis(2-ethanesulfonic acid); PMSF, phenylmethylsulfonyl fluoride; RNAi, RNA interference; SDS−PAGE, sodium dodecyl sulfate−polyacrylamide gel electrophoresis; UTR, untranslated region; VE-DIC, video-enhanced differential interference contrast.

10.1021/bi048157h CCC: $30.25
Published on Web 04/06/2005

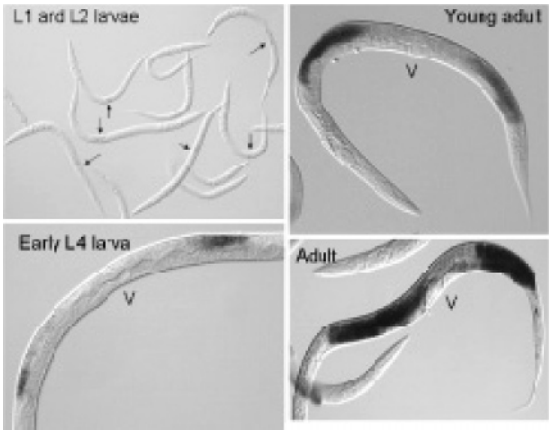

FIGURE 1: Expression patterns of klp-15 and/or klp-16 genes during development. Images obtained by in situ hybridization to klp-15/klp-16 mRNA. The mRNA for these two kinesin-14s is indistinguishable and is enriched in the two germline cells in L1 larvae (arrows). From the early L4 larval stage to young adults, expression is maximal in the late pachytene of meiosis I. It appears to spread to the diakinesis region in older adults. The V indicates the vulva and labels the ventral side of the animal.

and lengths of the introns and exons in the klp-15 and klp-16 genes are identical, except for a single base pair insertion and a single base pair deletion in two introns. The homology even extends to the promoter area, with 89% identity over the 131 bp immediately upstream of the genes. In practice, the sequence similarity of the two genes will prevent selective targeting of one or the other by RNA interference, cosuppression, or RNA hybridization.

The most obvious consequences of RNAi with either klp-15 or klp-16 are defects in meiosis (*16*−*19*) [see the movies at http://www.RNAi.org (*20*)]. Normally, *C. elegans* oocytes are arrested in the prophase of meiosis I, and this block is released at fertilization when the diploid and haploid products of meiosis I and II are ejected outside of the embryo as polar bodies. Inhibition of KLP-15/KLP-16 function, obtained by RNA_i or cosuppression, results in failure in meiotic spindle assembly, and consequently leads to defects in meiotic chromosome segregation. The meiotic prophase nuclei appear to be normal, and homologues are paired and attached by chiasmata; however, the polar bodies are abnormal in number or size, and correlatively the female pronucleus may also be of abnormal size. Probably as a result of aneuploidy, multiple nuclei sometimes form in one, two, and four cell embryos. Finally, an excess of males (X0) is observed among the few survivors, and this also indicates defective meiotic chromosome segregation. Interestingly, these defects are closely similar to those of a number of other essential genes that form a functional cluster that is active during meiosis and mitosis, in particular, cyclin B and the *Drosophila* abnormal spindle homologue. In situ hybridization shows that klp-15 and/or klp-16 mRNAs are concentrated in the germline at all stages, from L1 to adult (Figure 1). In L3, L4, and very young adults, transcripts accumulate in a specific region of the gonad, dorsal, and preturn, corresponding to the prophase of meiosis I, after the synaptonemal complex has been assembled, during pachytene. In older adults, the transcripts spread to the ventral gonad and are also present in large amounts in very early embryos. We conclude that the klp-15 and klp-16 genes are essential for acentriolar meiotic spindle formation and proper chromosome segregation.

KLP-15 and KLP-16 are predicted to have three structural domains: an N-terminal globular tail domain (residues Met1−Pro148), an α-helical coiled-coil region (residues Ser149−Leu246), potentially leading to dimerization or higher oligomers, and a globular C-terminal motor domain (Ile249−Val572), including the ATP-binding and MT-interaction sites. Previous studies on kinesin-1s, the conventional kinesins with the motor domain close to the N-terminus, have indicated that the α-helical coiled-coil domain is important for dimerization and strongly influences the kinetic properties of these kinesins. Curiously, the dimerization of the kinesin-14 subfamily has never been studied in any detail, and because of their small size, KLP-15/16 kinesins might possibly function as either dimers or monomers. Consequently, to initiate studies of these kinesins, we have cloned, expressed, and purified several KLP-15 constructs covering the motor domain and various lengths of the putative coiled-coil domain. These constructs have a His tag at their N-termini to facilitate purification and motility studies. We have examined the oligomeric state of these proteins, their in vitro ATPase kinetics, their microtubule binding, and finally their motility and directionality as determined by microtubule gliding observations.

EXPERIMENTAL PROCEDURES

Materials. The Rapid Excision Kit, the QuikChange Site-Directed Mutagenesis Kit, and Epicurean Coli XL10 Gold cells were obtained from Stratagene. Synthetic oligonucleotides were bought from MWG-Biotech AG. The Taq PCR Master Mix Kit for PCR, the plasmid DNA purification kit, the Ni−NTA conjugate, and Ni−NTA were purchased from Qiagen. Restriction enzymes were bought from NEB Biolabs. The Rapid DNA Ligation Kit was from Boehringer. The enzymes for kinetic assays and anti-His tag antibodies for microtubule gliding assays (catalog no. H1029) were from Sigma. Cover slips (superfrost plus, 22 mm × 75 mm × 1.0 mm, catalog no. 041300) for gliding assays were bought from Menzel Glazer. Beef tubulin for gliding assays and rhodamine-labeled tubulin were purchased from Cytoskeleton.

Cloning of KLP-15 Constructs. The cDNA clone yk 1466a11, encoding the entire KLP-15 protein, was obtained from Y. Kohara (National Institute of Genetics, Mishima, Japan). The insert was excised from the viral genome (λ ZAPII phage suspension) and cloned into the pbluescript vector using XPORT and XLOLR phages as described by the manufacturers. Potential monomeric and dimeric KLP-15 proteins were designed by aligning the protein sequence with *D. melanogaster* ncd. Unique restriction sites were introduced into the forward (NheI) and reverse primers (NotI) to allow subsequent cloning into *Escherichia coli* pET expression vectors. The corresponding DNA constructs were synthesized using the polymerase chain reaction. The following forward primers were used: A (klp-$15_{239-587}$), 5′-GAGTTGAGAAAGTTGGCTAGCGATGTTGTCGATTTA-3′; B (klp-$15_{215-587}$), 5′-AAAGTGGAGGAGTGCGCTAGCTATCGTGTGCACAAC-3′; C (klp-$15_{200-587}$), 5′-TCACTGCAAGATCAAGCTAGCACGCTGAAAGAAGTC-3′; D (klp-$15_{185-587}$), 5′-CAAATCCTGGATGGCGCTAGCGAAGGAGCGGATCGC-3′; and E (klp-$15_{148-587}$), 5′-CAGAAGCCTATTCTCGCTAGCAAGATGGCGCTTCTT-3′.

The following reverse primer was used in all cloning strategies: O, 3′-TACAGATACTTGATCCGCCGGCGAAGATAAGATTGTAAA-5′. The resulting PCR products were digested using NheI and NotI restriction enzymes, gel purified, isolated, and ligated into expression vectors, previously restricted with the same enzymes. Fragment B was cloned into pET17b (ampicillin resistant), whereas fragments A and C−E were ligated into pET28a, which carries the resistance for kanamycin. Fragments A and C−E automatically carried a coding sequence for six histidine residues at the N-terminus of the protein, since pET28a carries a start codon and a His tag coding sequence upstream of the NheI restriction site. Fragment B required a second cloning step for the incorporation of the histidine tag into the coding sequence. For this purpose, the three plasmids were digested with NheI and the resulting sticky ends dephosphorylated. The following forward and reverse primers encoding six histidines were ligated into the linearized vector: 5′-CTAGCCACCACCACCACCACCACCCATGGG-3′ and 3′-GGTGGTGGTGGTGGTGGTGGGTACCCGATC-5′. Positive clones containing the desired insert were identified by double restriction with NheI and NotI, and the correctness of the cloning strategy was confirmed by DNA sequencing of all the constructs.

Expression and Purification of Protein Constructs. All KLP-15 proteins were purified at 4 °C using the same batch protocol. We optimized the expression of the different constructs by testing several *E. coli* strains, IPTG concentrations, and expression temperatures and times. Cells were harvested, frozen in liquid nitrogen, and stored at −80 °C. For protein purification, the cells were thawed and resuspended in buffer A [50 mM NaH_2PO_4/Na_2HPO_4 (pH 7.5), 4 mM $MgCl_2$, 300 mM NaCl, 10% glycerol, 5 mM imidazole (pH 7.5), 0.1 mM Na-EGTA, and 5 mM β-ME]. Cells were lysed twice in the presence of 1 mM PMSF, 1 mM ATP, and 40 μg/mL DNAse using a French press. The lysate was centrifuged at 48000*g* for 20 min, and the supernatant was incubated for 1 h with 5 mL of Ni−NTA resin previously equilibrated with buffer A. The Ni−NTA batches were washed at least four times with buffer B [20 mM PIPES (pH 7.0), 4 mM $MgCl_2$, 200 mM NaCl, 5% glycerol, 40 mM imidazole (pH 7.5), and 5 mM β-ME]. The Ni−NTA resin with bound KLP-15 protein was poured into small columns and the protein eluted with buffer C [20 mM PIPES (pH 7.0), 4 mM $MgCl_2$, 30 mM NaCl, 5% glycerol, 200 mM imidazole (pH 7.5), and 5 mM β-ME], taking fractions of 1 mL. The fractions containing the protein were concentrated to ∼20 mg/mL using a CENTRICON-30 and applied to a gel filtration column, previously equilibrated in buffer D [30 mM PIPES (pH 7.0), 1 mM $MgCl_2$, 30 mM NaCl, 1 mM Na-EGTA, and 1 mM DTT]. The peak fraction was pooled, concentrated, frozen in liquid nitrogen, and stored at −80 °C until it was used.

The protein concentration was measured by using the theoretical extinction coefficients calculated from the primary protein sequence using ProtParam (*21*) (http://au.expasy.org/tools/protparam.html) (20 340 M^{-1} cm^{-1} for KLP-$15_{239-587}$, 27 310 M^{-1} cm^{-1} for KLP-$15_{215-587}$, 21 620 M^{-1} cm^{-1} for KLP-$15_{200-587}$, 21 620 M^{-1} cm^{-1} for KLP-$15_{185-587}$, and 21 620 M^{-1} cm^{-1} for KLP-$15_{148-587}$). To release bound ADP that also contributes to the extinction coefficient (*22*), 100 μL of each KLP-15 protein was precipitated using 7% perchloric acid and incubated for 5 min on ice. We assume that no cystine (S−S) is present in KLP-15, and therefore, cysteine residues present in the primary sequence do not contribute to the extinction coefficient. After centrifugation, the pellets were resuspended in 6.0 M guanidine hydrochloride and 200 mM phosphate buffer (pH 6.5) and the absorption was measured at 280 nm. Further analysis of the supernatants showed that all the protein was precipitated, and the ADP that was released corresponded to one ADP per site (data not shown).

The Bradford method (*23*) was used to calibrate each construct with known concentrations measured with the method described above. Five replicates per construct were averaged. The tubulin concentration was determined by the absorbance at 275 nm in 6 M guanidine hydrochloride, using an extinction coefficient of 1.03 mL mg^{-1} cm^{-1} (*24*). The concentration is expressed in tubulin dimers (110 kDa).

The coupled ATPase activity test with ATP regeneration (*24*) was used to study the enzymatic characteristics of KLP-15. The basal ATPase activity was measured at KLP-15 concentrations between 1 and 3 μM, and the MT-activated ATPase activity was determined at a protein concentration of ∼0.5 μM.

Analytical Ultracentrifugation. A Beckman Optima XL-I analytical ultracentrifuge equipped with an An-60 Ti rotor was used to perform sedimentation velocity experiments at 60 000 rpm (∼300000*g*) at a temperature of 10 °C in 20 mM PIPES (pH 7.3), 30 mM NaCl, 1 mM $MgCl_2$, 1 mM Na-EGTA, 1 mM DTT, 1 mM NaN_3, and 10 μM MgATP. The five different KLP-15 proteins were investigated at various concentrations. The cells were equipped with quartz windows with, for protein concentrations between 0.5 and 1 mg/mL, 12 mm optical path central pieces of 440 μL and, for higher protein concentrations, 3 mm optical path central pieces of 110 μL. Before each run, the diluted protein was incubated overnight at 4 °C in the cell, to reach the dissociation equilibrium. For each construct and measurement, the wavelength was individually adjusted in the range of 265−272 nm. The Sedfit program package (http://www.analyticalultracentrifugation.com) was used to analyze the sedimentation profiles in terms of either a continuous distribution of the sedimentation coefficient $c(s)$ (*25*) or one or two discrete, noninteracting, species (*26*). Sedfit also incorporates a systematic noise evaluation procedure (*27*). We used the Sednterp software to estimate the partial specific volumes of the KLP-15 constructs (0.7240−0.7258 mL/g) and the density (1.00183 mL g^{-1}) and viscosity (0.013207 mPa s) of the solvent (Sednterp version 1.01; developed by D. B. Haynes, T. Laue, and J. Philo; http://www.bbri.org/RASMB/rasmb.html), which were used to calculate normalized coefficients ($s_{20,w}$) from the experimental sedimentation coefficients (s). For the $c(s)$ analysis, we typically used 70 experimental profiles obtained every 5 min. We considered 200 particles with a frictional ratio (f/f_0) of 1.5, with sedimentation coefficients between 1 and 6 S, and used a grid of 500 radial points and a confidence ratio of 0.68 for the regularization procedure. The $c(s)$ distributions were then fitted to one or two Gaussians to provide values for the sedimentation coefficients and for the relative concentrations of the species. In our specific experiments, we have to consider essentially two species, namely, monomers and

dimers. These are considered to be noninteracting if there is no monomer association or dimer dissociation over the time scale of the experiment. Analysis in terms of the one or two noninteracting component model gives direct fits for the values of s, M_w, and concentration. Equilibrium dissociation constants, K_d, were calculated using eq 1 to fit the measured dimer percentage (% dimer) as a function of the total protein concentration, C_{total}.

$$\%\ \text{dimer} = 100[K_d + 4C_{total} - (K_d^2 + 8K_dC_{total})^{1/2}]/(4C_{total}) \quad (1)$$

This equation is obtained from the following definitions where subscripts indicate total, monomer, and dimer concentrations:

$$K_d = C_{monomer}^2/C_{dimer};\ C_{total} = C_{monomer} + 2C_{dimer};\ \%\ \text{dimer} = 100(2C_{dimer}/C_{total})$$

Pelleting Assays. Pelleting assays were performed as described previously (*28*). Tubulin and KLP-15 concentrations were determined as described above. Experiments in the presence of either ADP or AMPPCP were carried out at a KLP-15 concentration of 4 μM and with tubulin concentrations between 0 and 40 μM. The final volume of the reaction solution was 48 μL in PEM buffer supplemented with 1 μM taxol, 4 mM magnesium acetate, and 3 mM nucleotide (ADP or AMPPCP). KLP-$15_{215-587}$ precipitated at higher AMPPCP concentrations. To improve stability, KLP-$15_{215-587}$ was stored in the presence of at least 50 μM MgATP. For the pelleting experiment, the protein was diluted five times to give a final MgATP concentration of 10 μM. Thus, experiments performed in the "absence of nucleotide" contain a maximal MgATP concentration of 10 μM. We used NIH image (http://rsb.info.nih.gov/nih-image) for the quantitative analysis of bound and unbound kinesin concentrations. Protein concentrations were determined from the intensity of the bands in the SDS−PAGE gel by calibrating against a range of known KLP-$15_{215-587}$ concentrations.

The binding stoichiometry of the monomeric KLP-$15_{215-587}$ and microtubules, along with the dissociation constant, was determined by plotting the KLP-$15_{215-587}$ concentration cosedimenting with microtubules as a function of total microtubules (expressed as tubulin dimer concentration). Mutual depletion was taken into account by fitting the plot with the following equation (*28*, *29*):

$$MtN = (N/2N_0)[A - (A^2 - 4N_0Mt_0)^{1/2}] \quad (2)$$

where N/N_0 is a normalizing factor (corresponding to the maximum fraction of kinesin binding to microtubules), $A = K_d + Mt_0 + N_0$, MtN is the concentration of KLP-15 bound to microtubules, N is the maximum concentration of bound KLP-15, N_0 is the total KLP-15 concentration, Mt_0 is the total tubulin concentration, and K_d is the apparent dissociation constant.

In Vitro Microtubule Gliding Assays. Gliding assays were performed by binding purified KLP-15 via the N-terminal His tag to anti-His antibodies attached to the glass coverslip of the perfusion chambers. KLP-15 was transferred into buffer E [10 mM imidazole (pH 7.5), 2 mM magnesium formate, 50 mM NaCl, 1 mM Na-EGTA, 1 mM DTT, and 4 mM MgATP] by gel filtration. Then 20 μL of anti-His tag antibodies at a concentration of ~10 μM in buffer E was injected into the perfusion chamber and incubated for 5 min. The chamber was washed with 20 μL of buffer E, and then 20 μL of KLP-15 at 30 μM in buffer E was injected and incubated for 10 min. After the chamber had been washed with 20 μL of buffer E, MTs were injected at a concentration of 1 μM in buffer E. Finally, the chamber was washed with buffer E supplemented with 10 μM paclitaxel and placed on the microscope to record MT gliding.

We used a VE-DIC microscope equipped with a 1.4 NA objective with a magnification of 100× and a Cohu CCD camera. The microscope was maintained at 20 °C in a temperature-controlled room. Image treatment (background subtraction, signal-to-noise improvement) was performed using an Argus-20 Hamamatsu image processor. MT movement was recorded on digital DVCAM recording media. A *Neurospora crassa* conventional kinesin construct, Nkin460-GST (*30*), whose gliding velocity has been previously established (*31*), was used as a positive control. This protein is stable at room temperature. Nkin460GST was purified as described previously (*31*).

MT gliding velocities V (micrometers per second) were determined from the video recordings using NIH image software with some in-house modifications of existing macros. The coordinates of selected MT extremities were obtained using the computer cursor and together with the acquisition times of successive images were exported into Excel. Gliding velocities V were calculated using the following equation:

$$V = 25E \times \text{shift}/(N_2 - N_1) \quad (3)$$

where $\text{shift} = \sqrt{[(x_2 - x_1)^2 + (y_2 - y_1)^2]}$ is the displacement calculated from the pixel coordinates (x_1,y_1) and (x_2,y_2) of a MT extremity in image numbers N_1 and N_2, respectively. The recording rate was 25 images per second, giving a time delay of $(N_2 - N_1)/25$ between images N_1 and N_2. The scale factor E converts the shift from pixels into micrometers (10 μm corresponds to 97 pixels both horizontally and vertically on the CCD camera).

The direction of movement along microtubules was determined by a modified protocol, originally described by Hyman, using microtubules with rhodamine-labeled minus ends (*32*, *33*).

RESULTS

Five KLP-15 proteins were expressed and purified (Figure 2a,b). As shown in Table 1, the calculated molecular masses derived from the KLP-15 primary sequence agree with the masses measured by MALDI mass spectrometry. Using gel filtration, we estimated that KLP-$15_{239-587}$ is a monomer whereas KLP-$15_{215-587}$, a construct including a longer portion of the predicted coiled-coil domain (Figure 2c), elutes with a double peak, possibly indicating a monomer−dimer equilibrium (data not shown). The longer KLP-15 constructs appear to be dimers. The oligomeric state of the five KLP-15 constructs was examined in more detail by sedimentation velocity experiments as described below.

Hydrodynamic Properties. A typical set of measured sedimentation profiles and calculated fits is shown in Figure

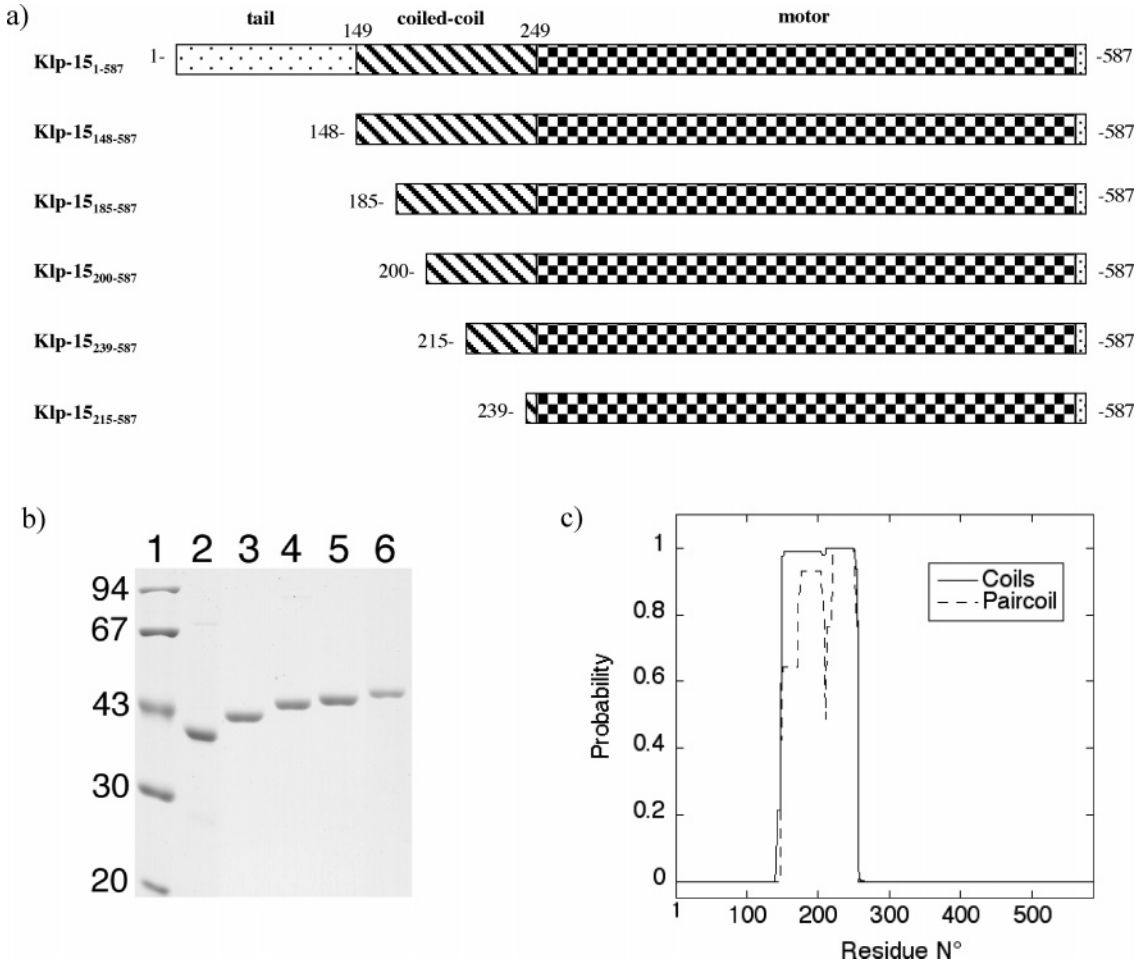

FIGURE 2: *C. elegans* KLP-15 constructs. (a) The N-terminal tail domain of KLP-15 (residues Met1−Pro148) is followed by a continuous α-helical region (residues Ser149−Leu246) predicted to form a coiled coil leading to dimerization. The C-terminal motor domain (residues Ile249−Val572) contains the ATP-binding and MT-interacting sites. The KLP-15 proteins investigated contain the motor domain and varying numbers of residues in the α-helical region, as shown. (b) SDS−PAGE of purified KLP-15 proteins: lane 1, standard protein markers; lane 2, KLP-15$_{239-587}$; lane 3, KLP-15$_{215-587}$; lane 4, KLP-15$_{200-587}$; lane 5, KLP-15$_{185-587}$; and lane 6, KLP-15$_{148-587}$. (c) Coiled-coil regions in KLP-15 as predicted by COIL (*50*) and PAIRCOIL (*51*).

Table 1: Summary of the Physical Properties of KLP-15 Constructs[a]

KLP-15 construct	predicted no. of amino acids in coiled coil	N-terminal sequencing	calculated molecular mass[b] (Da)	measured molecular mass[c] (Da)	estimated molecular mass (kDa)[d]	association state[e]
KLP-15$_{239-587}$	7	*GSSHHHHHHSSGLVPRGSHMASDVV	40 408	40 479		monomer
KLP-15$_{215-587}$	31	*ASHHHHHHPWASYRV	42 481	42 416	44/97	monomer + dimer
KLP-15$_{200-587}$	46	nd[f]	45 097	45 143	75	monomer + dimer
KLP-15$_{185-587}$	61	nd[f]	46 752	46 819	88	monomer + dimer
KLP-15$_{148-587}$	97	nd[f]	50 864	50 839	94	dimer

[a] The initial methionine residue is missing due to N-terminal excision in *E. coli* (*49*) as shown by N-terminal sequencing. Klp15 constructs cloned into pET17 start with an Ala, whereas constructs cloned into pET28 start with a Gly. [b] Calculated from the primary sequences. The additional N-terminal residues, including the linker, the His tag (ASHHHHHHPWAS or GSSHHHHHHSSGLVPRGSHMAS), and missing methionine residues, are taken into account. [c] Determined by MALDI-TOF. [d] Estimation of molar mass determined by FPLC gel filtration on a Superose 12 column. [e] From analytical ultracentrifugation sedimentation velocity experiments. [f] Not determined.

3. Figure 4a−e shows the distribution of sedimentation coefficients of the KLP-15 constructs for different protein concentrations. The shortest and longest constructs (KLP-15$_{239-587}$ and KLP-15$_{148-587}$, respectively) show single peaks, with $s_{20,w}$ values of 3.0 and 4.3 S, respectively, the positions of which do not change significantly in the investigated range of protein concentrations. This suggests that the shortest construct with 348 amino acid residues (KLP-15$_{239-587}$) is monomeric and the longest with 439 residues (KLP-15$_{148-587}$) is dimeric. The sedimentation coefficient ($s_{20,w}$ = 3.0 S) for KLP-15$_{239-587}$ is consistent with values previously reported for kinesin monomer constructs such as *D. melanogaster* ncd (MC6) with 367 residues (3.31−3.7 S) (*28*, *34*) and conventional kinesins with 340 (3.25 S) and 341 residues (2.9 S) (*35*−*36*). The sedimentation coefficient ($s_{20,w}$ = 4.3 S) of KLP-15$_{148-587}$ can be compared to the values of 4.9 and 5.0 S found for dimeric ncd MC1 with 491 residues (there are 13 additional residues at the N-terminus due to the expression system) and with the values of 5.18 and 5.06 S for conventional kinesin constructs with 392 and 401

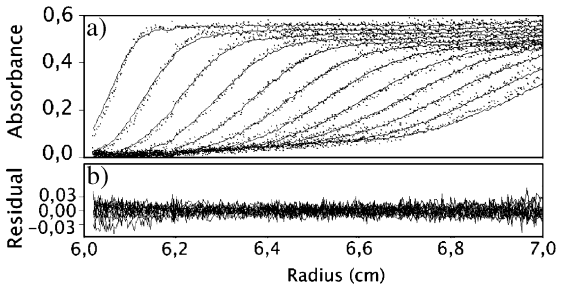

FIGURE 3: Sedimentation velocity profiles of KLP-$15_{200-587}$. (a) Twelve profiles obtained at 0.5 mg/mL, 10 °C, and 60 000 rpm. Each dotted curve shows the measured absorbance at 276 nm as a function of the distance from the rotation axis. The *c*(*s*) analysis fits are shown as continuous lines. (b) The residuals show the differences between the experimental and fitted sedimentation profiles.

residues, respectively. The intermediate-length KLP-15 constructs show two $s_{20,w}$ peaks positioned at 2.7−3.0 and 3.7−4.3 S. Analyzing the data by the alternative noninteracting particle model gives essentially the same results, indicating that the sediment coefficients are in fact consistent with a monomer and a dimer species (Table 2). For constructs KLP-$15_{215-587}$, KLP-$15_{200-587}$, KLP-$15_{185-587}$, and KLP-$15_{148-587}$, the analysis gives molar masses for the monomer and dimer in solution that are within 10% of the theoretical values (data not shown). Furthermore, the ratio of the $s_{20,w}$ values for the dimer and monomer (1.51 ± 0.04) agrees with the theoretical value of 1.5 calculated for an assembly of two globular monomers (*37*). Figure 4f shows that in solution, the intermediate-length constructs consist of both monomeric and dimeric proteins in slow equilibrium, and the longest and shortest constructs are monomeric and dimeric, respectively. Dissociation constants K_d, calculated using eq 1, are listed in Table 3 and are plotted against predicted coiled-coil lengths of the different constructs in Figure 4g.

ATPase Activity. The enzymatic characteristics of the KLP-15 constructs are summarized in Table 4. In the absence of salt, all constructs have similar basal ATPase activities per motor domain, varying from 0.025 to 0.031 s^{-1}. The basal ATPase activity is stimulated by a factor of up to 2 in the presence of 300 mM NaCl (Figure 5a). In the presence of microtubules, the ATPase activity of the constructs is in the range of 2.8−4.0 s^{-1}, showing that ATP hydrolysis is stimulated by a factor of 100−150 in the presence of MTs (Figure 5b and Table 4). This stimulation is highly dependent on salt concentration (Figure 5c).

Steady-State Binding to Microtubules. Kinesins are thought to move along microtubules via a cycle of coupled changes in conformation and microtubule affinity that are related to ATP turnover. We investigated the binding characteristics of KLP-$15_{215-587}$ by varying the microtubule concentration (from 0 to 40 μM) at a fixed KLP-15 concentration (4 μM) in the presence of either ADP or AMPPCP (nonhydrolyzable ATP analogue) and without added nucleotide. After incubation, the solutions were centrifuged and the supernatants and pellets analyzed by SDS−PAGE. KLP-$15_{215-587}$ and tubulin are well resolved on the gels (Figure 6a), whereas the bands from longer KLP-15 constructs overlap with those of tubulin. The intensities of the bands from the supernatant and pellet were measured by densitometry. The data presented in Figure 6b show that under all nucleotide conditions, the totality of the kinesin binds to microtubules at saturation. K_d values obtained by fitting the data to eq 2 (Figure 6c) show that the weakest microtubule binding state occurs in the presence of ADP.

Microtubule Gliding and Direction of Movement. We first determined the gliding velocities for the *N. crassa* kinesin construct Nkin460GST and obtained an average gliding velocity of 101 ± 3 μm/min from measurements on 67 MTs. Within the experimental error, this is identical to the previously determined value of 108 ± 12 μm/min for this construct (*31*). A gliding velocity of 156 ± 30 μm/min was previously obtained for the full-length protein with 928 amino acids purified from wild-type 74A *N. crassa* cell cultures (*33*, *38*).

All five KLP-15 constructs were tested for their ability to induce MT gliding. We attached anti-His tag antibodies to the coverslip of the motility chamber to enable the KLP-15 constructs to interact with the antibody by their N-terminal His tag. All constructs, except KLP-$15_{239-587}$, showed MT gliding for up to 30 min, in agreement with our observation that, at room temperature, KLP-15 loses its ATPase activity on a similar time scale. Microtubules themselves were stable over this time scale, as verified by length measurements. We also checked that, in the absence of KLP-15, there were very few microtubule interactions with the glass surface of the motility chamber both in the absence and in the presence of the anti-His tag antibody. The results shown in Figure 7 were obtained with KLP-$15_{148-587}$, the longest construct containing the motor domain and the entire predicted coiled-coil domain. The average MT gliding velocity for this construct was 2.3 ± 0.3 μm/min (32 individual microtubules were observed), placing KLP-15 among the low-velocity kinesins.

The direction of movement along microtubules was determined by fluorescence microscopy using microtubules with rhodamine-tubulin labeled minus ends (*32*, *33*). The five KLP-15 constructs were tested, and again, no movement could be detected for KLP-$15_{239-587}$; on the other hand, all of the other constructs induced MT gliding. Out of 22 rhodamine-labeled MTs that were studied, all moved as shown in Figure 8, indicating that KLP-15 moves toward MT minus ends, like other kinesin-14s studied to date.

DISCUSSION

KLP-15 constructs cloned into pET expression vectors and expressed in *E. coli* produced soluble, active, and easily purified recombinant proteins. Molecular masses as determined by mass spectrometry agree with calculated values based on primary sequences (Table 1).

The dimerization of a member of the kinesin-14 subfamily is examined in detail for the first time. The length of the α-helical region preceding the NH_2-terminal end of the motor domain is found to strongly influence the dimerization of *C. elegans* KLP-15. A construct with seven residues in the predicted α-helical coiled-coil region, KLP-$15_{239-587}$, is monomeric in solution. The construct, KLP-$15_{148-587}$, with the complete predicted coiled-coil region containing 97 residues, is a stable dimer. Intermediate-length constructs, at concentrations in the milligram per milliliter range, consist of monomers and dimers in (slow) equilibrium, allowing the dissociation constants K_d to be determined (Table 3). A plot

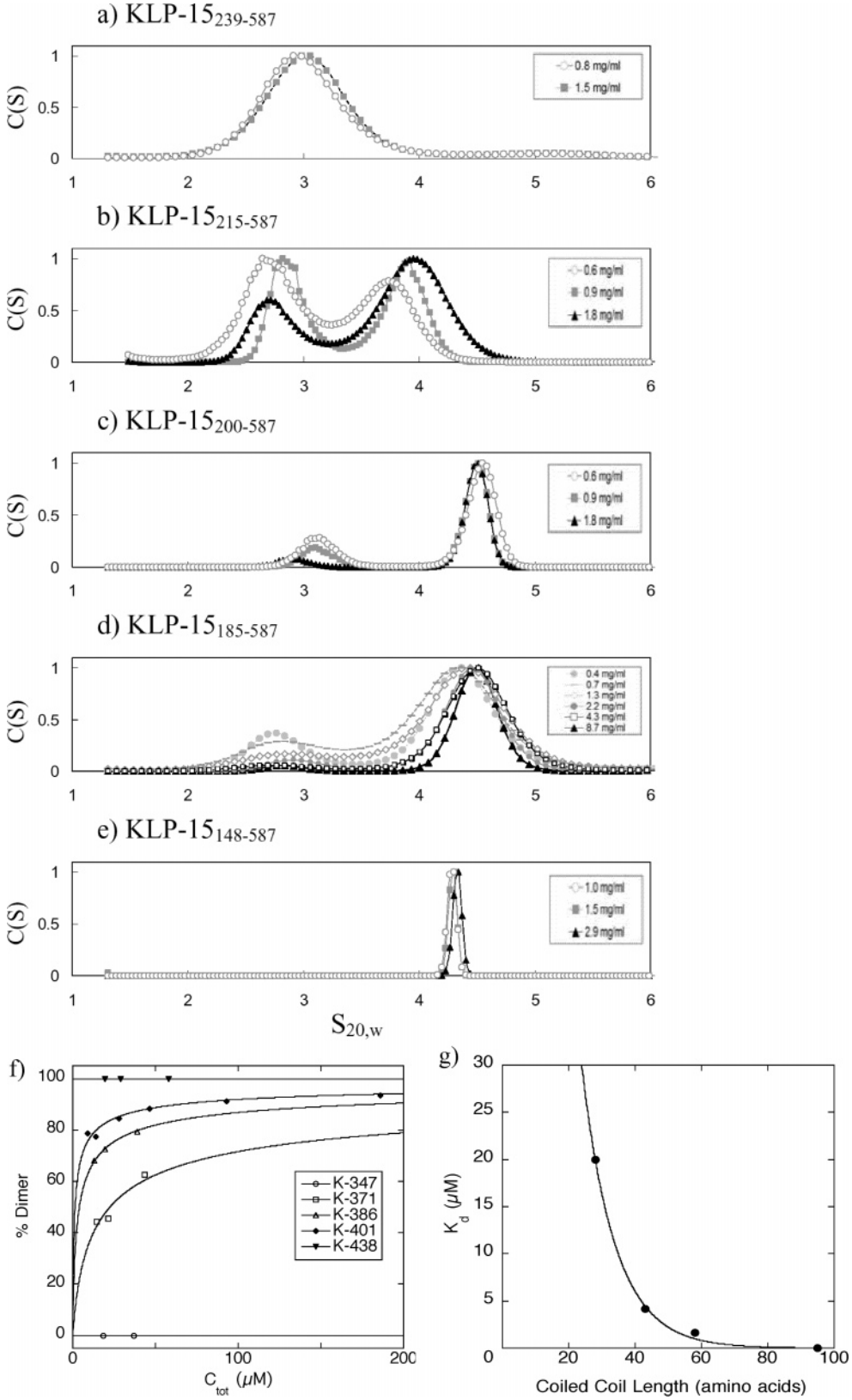

FIGURE 4: Sedimentation velocity analysis of the five KLP-15 constructs. Distribution (arbitrary units) of sedimentation coefficients $s_{20,w}$ for (a) KLP-$15_{239-587}$ at 0.8 and 1.5 mg/mL, (b) KLP-$15_{215-587}$ at 0.6, 0.9, and 1.8 mg/mL, (c) KLP-$15_{200-587}$ at 0.6, 0.9, and 1.8 mg/mL, (d) KLP-$15_{185-587}$ at 0.4, 0.7, 1.3, 2.2, 4.3, and 8.7 mg/mL, and (e) KLP-$15_{148-587}$ at 1, 1.5, and 2.9 mg/mL. For panels b−d, a larger proportion of the dimer species is obtained at the higher concentrations. (f) Percentage of dimer shown as a function of the total concentration for each construct. (g) Dissociation constants as a function of the predicted coiled-coil length.

of K_d as a function of the number of amino acids (L) in the predicted coiled coil (Figure 4g) is fitted by an exponential curve of the form $K_d = A \exp(-\lambda L)$, where $\lambda = 0.1$. In this expression, K_d is halved for each additional seven amino acids in the coiled-coil region. Since the construct with the full-length predicted coiled-coil region forms a stable dimer,

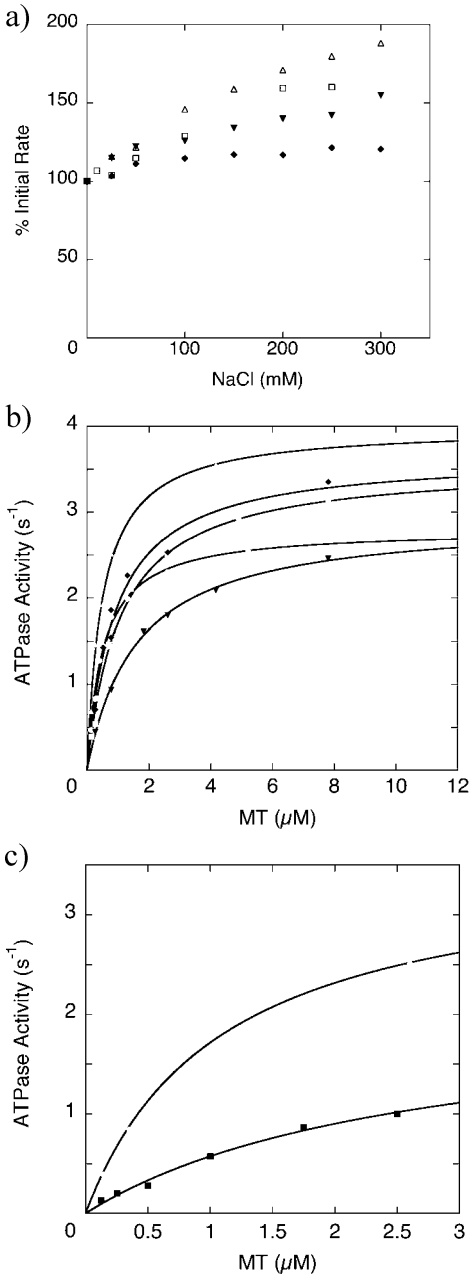

FIGURE 5: ATPase activity of KLP-15. (a) Salt dependence of the basal ATPase activity: KLP-$15_{215-587}$ (□), KLP-$15_{200-587}$ (△), KLP-$15_{185-587}$ (◆), and KLP-$15_{148-587}$ (▼). The ATPase is stimulated by a factor of up to 2 in the presence of 300 mM NaCl. (b) Steady-state measurements of the MT-activated ATPase activity: KLP-$15_{239-587}$ (○), KLP-$15_{215-587}$ (□), KLP-$15_{200-587}$ (△), KLP-$15_{185-587}$ (◆), and KLP-$15_{148-587}$ (▼). (c) Effect of salt on the microtubule-stimulated ATPase activity of KLP-15: no salt (○) or in the presence of 50 mM NaCl (■). The values for kinetic constants k_{cat} and $K_{0.5}$ are summarized in Table 4.

native KLP-15 is likely to be active in vivo as a dimeric protein. The complete α-helical coiled-coil stalk is estimated to have 97 amino acids. This is equivalent to ~14 heptad repeats and, on the basis of a rise of 1.05 nm per repeat, corresponds roughly to a length of 15 nm. No higher-order oligomers were observed even at the relatively high concentrations used for the analytical centrifugation. These results contrast with those obtained for conventional kinesin where a region some 40 amino acids in length was found to be sufficient to produce a stable coiled coil leading to a fully functional dimeric protein (*35*, *39*, *40*).

Table 2: Sedimentation Velocities of KLP-15 Constructs[a]

protein	concentration (mg/mL)	$s_{20,w}$ (*S*) monomer	$s_{20,w}$ (*S*) dimer	dimer (%)
KLP-$15_{239-587}$	0.75	3.02	–	0
	1.50	2.96	–	
	–	–	–	
KLP-$15_{215-587}$	0.61	2.72	3.70	46
	0.92	2.86	3.88	53
	1.84	2.74	3.95	70
KLP-$15_{200-587}$	0.58	2.78	4.50	79
	0.88	2.94	4.51	80
	1.75	2.53	4.52	91
KLP-$15_{185-587}$	0.44	2.91	4.33	73
	0.66	2.78	4.37	75
	1.32	3.02	4.42	78
	2.17	3.02	4.42	89
	4.43	2.91	4.33	91
	8.67	2.78	4.37	95
KLP-$15_{148-587}$	0.98	–	4.28	100
	1.47	–	4.29	
	2.89	–	4.29	

[a] The sedimentation coefficients and relative proportions of the monomer and dimer were determined using the model of one or two noninteracting species, as described in the text.

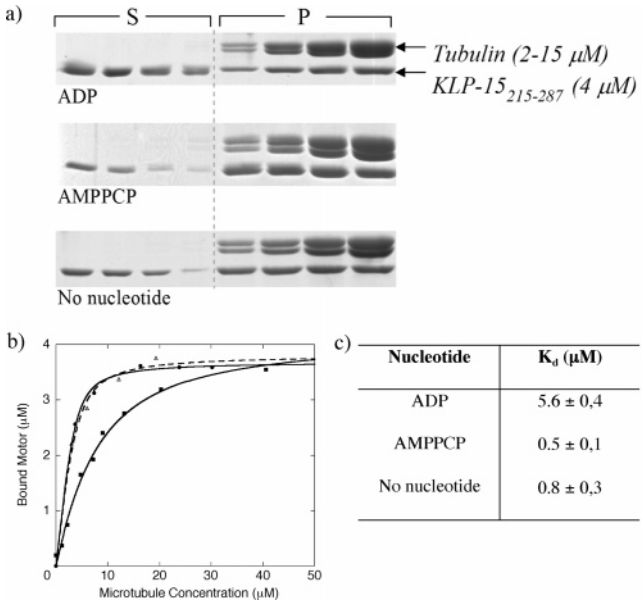

FIGURE 6: Microtubule affinity of KLP-15. (a) SDS−PAGE of the supernatant (S) and pellet (P) after centrifugation of KLP-15 in the presence of microtubules at increasing concentrations from lane 1 (2 μM) to lane 4 (15 μM) and in the presence of ADP, AMPPCP, and no added nucleotide as indicated. (b) Bound KLP-15 as a function of microtubule concentration in the presence of ADP (■), without nucleotide (△), and AMPPCP (●). (c) Dissociation constants K_d in the presence of microtubules taking mutual depletion into account (eq 2).

Microtubules stimulate the ATPase activity of all KLP-15 constructs by a factor in the range of 100−150. The basal and microtubule-stimulated ATPase activities are similar for all constructs, whereas for another kinesin-14, *D. melanogaster* ncd, monomers are stimulated considerably more than dimers (*34*). The k_{cat} values of 2.8−4.0 s^{-1} in the presence of microtubules are in good agreement with the previous results for other kinesin-14s: k_{cat} varies from 0.2 to 3.8 s^{-1} for different constructs of ncd (*34*), from 1.7 to 2.2 s^{-1} for the ncd motor domain (*41*), and from 1.8 to 2.0 s^{-1} for a long dimeric ncd construct MC1 (*28*). A value of 0.5 s^{-1} was obtained for the motor domain of *S. cerevisae* Kar3 (*42*). Thus, the values for kinesin-14s are consistently low

Table 3: Dissociation Constants of KLP-15 Constructs

	KLP-15$_{239-587}$	KLP-15$_{215-587}$	KLP-15$_{200-587}$	KLP-15$_{185-587}$	KLP-15$_{148-587}$
coiled-coil length, no. of amino acids[a]	7	31	46	61	97
K_d (μM)	∞	20 ± 2	4.18 ± 0.08	1.62 ± 0.02	0

[a] Predicted using PAIRCOIL (*51*).

Table 4: Enzymatic Properties of KLP-15 Constructs

protein	basal ATPase activity k_0 (s^{-1}) per motor domain[a]	MT-activated ATPase activity per motor domain		activation K_{cat}/k_0	$K_{bi} = k_{cat}/K_{0.5}$ (s^{-1} μM^{-1})
		k_{cat} (s^{-1})	$K_{0.5}$ (μM)		
KLP-15$_{239-587}$	0.026 ± 0.007	2.80 ± 0.08	0.52 ± 0.05	108	5.4
KLP-15$_{215-587}$	0.031 ± 0.001	3.56 ± 0.07	1.08 ± 0.07	116	3.3
KLP-15$_{200-587}$	0.031 ± 0.004	3.99 ± 0.08	0.50 ± 0.04	129	8.0
KLP-15$_{185-587}$	0.025 ± 0.002	3.67 ± 0.19	0.90 ± 0.13	148	4.1
KLP-15$_{148-587}$	0.028 ± 0.002	2.93 ± 0.07	1.58 ± 0.10	103	1.9

[a] In the absence of salt.

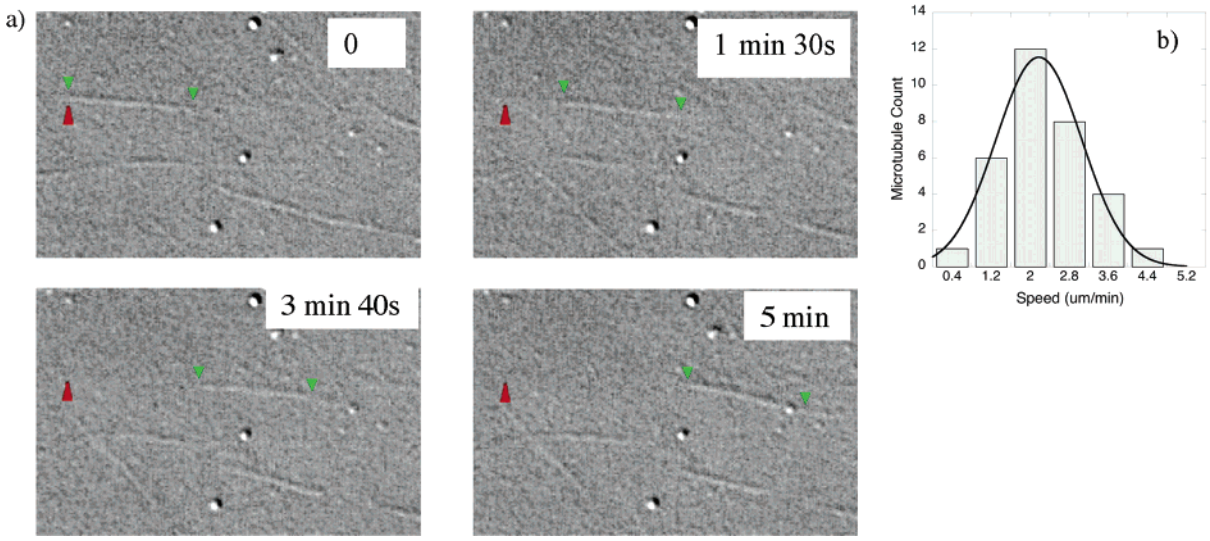

FIGURE 7: Dimeric KLP-15 supports microtubule movement. (a) Video-enhanced differential interference contrast microscopy observations of MT gliding. The surface of a coverslip was coated with KLP-15$_{148-587}$ as described. The images from the top left to bottom right represent a 5 min time series. Green arrowheads point to MT ends, and the red arrowhead indicates a fixed reference point. (b) Histogram showing the observed microtubule velocity distribution (gray bars). The full curve is a Gaussian regression applied to the histogram. The uncertainty over the average is calculated with a probability of 95%. The average velocity is 2.3 ± 0.3 μm/min.

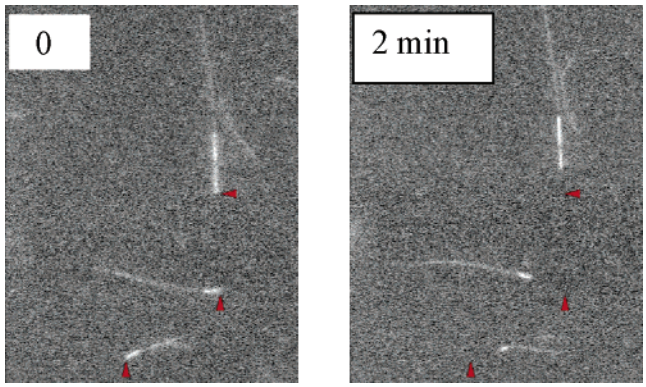

FIGURE 8: Dimeric KLP-15 moves to microtubule minus ends. Microtubule minus ends marked with rhodamine-labeled tubulin appear brighter than the rest of the microtubules. Fixed reference points are marked with red arrowheads.

compared to those of monomeric and dimeric kinesin-1 constructs, which typically have k_{cat} values between 38 and 96 s^{-1} (*39*).

MT gliding assays in the multimotor mode show that all the KLP-15 constructs with a dimeric component behave as slow motors (a value of 2.3 ± 0.3 μm/min was measured for the fully dimeric construct), whereas the monomeric construct is immobile under the same experimental conditions. Since our measured gliding velocities for *N. crassa* conventional kinesin (Nkin460GST) are in good agreement with previous measurements (*31*, *38*), we are confident in the gliding velocity found for KLP-15 obtained under the same conditions. We have confirmed that KLP-15 is a minus end-directed (retrograde) motor like other kinesin-14s examined to date. This is the third member of the kinesin-14 subfamily for which the gliding velocity has been determined using constructs that closely mimic the native protein. Bacterially expressed, full-length CHO2 gave microtubule gliding velocities of 1.1−5.2 μm/min (*43*); near-full-length ncd gave velocities of 1.5−7 μm/min (*44*), and a His-tagged ncd dimer attached to a metal chelating surface gave a gliding velocity of 9.6 ± 0.6 μm/min (*45*). GST fusion proteins have often been used in gliding assays to ensure that kinesin constructs attach in the correct orientation on the glass surface of the motility cell. For such constructs, the following gliding velocities have been reported: 0.5−8.4 μm/min for different CHO2 constructs (*43*), 5−10 μm/min for *D. melanogaster*

ncd (*34*), 8−10 μm/min for *Arabidopsis thaliana* KCBP (*46*), and finally 1−2 μm/min for *S. cerevisae* Kar3 (*47*). Thus, although GST fusion proteins may strongly influence dimerization, the gliding velocities of the fusion and "native" kinesin constructs are similar. KLP-15 and CHO2 appear to be the slowest kinesins examined to date. Overall, members of the kinesin-14 subfamily are slow motors compared to kinesin-1 (conventional kinesin) that moves 5−10 times more quickly.

Essential C-terminal kinesins KLP-15 and KLP-16 are the closest metazoan relatives to ncd in the entire kinesin-14 family tree (*14*). KLP-15 is required, by itself or in conjunction with KLP-16, for proper meiosis. The role of KLP-15 and/or KLP-16 in the assembly of the bipolar meiotic acentriolar spindle is consistent with the well-characterized role of the microtubule bundling nonclaret disjunctional (ncd) in the *Drosophila* female meiotic spindle (*48*).

In conclusion, *C. elegans* KLP-15 is likely to be a slow, dimeric kinesin in vivo. The almost identical KLP-16 is likely to share the properties determined for KLP-15. These two kinesins appear to be essential for germline function. Thus, either (or both) will be excellent models for in vivo investigations of the role of this kinesin-14 subgroup in cell division.

ACKNOWLEDGMENT

We thank Jean-Pierre Andrieu (IBS, Grenoble, France) for N-terminal sequencing of KLP-15 constructs and David Lascoux (IBS) for the MALDI mass spectrometry analysis. We thank Yuji Kohara (Genome Biology Lab, National Institute of Genetics, Mishima, Japan) for generously providing the cDNA encoding KLP-15. We also thank Isabelle Crevel, Fabienne Pirollet, and David D. Hackney for advice. Taxotere was a gift from Aventis.

REFERENCES

1. Schliwa, M., Ed. (2003) *Molecular motors*, Wiley-VCH, New York.
2. Thierry-Mieg, J., Thierry-Mieg, D., Potdevin, M., and Sienkiewicz, M. (2005) Identification and functional annotation of cDNA-supported genes in higher organisms using AceView, http://www.ncbi.nlm.nih.gov/IEB/Research/Acembly.
3. Koushika, S. P., and Nonet, M. L. (2000) Sorting and transport in *C. elegans*: A model system with a sequenced genome, *Curr. Opin. Cell Biol. 12*, 517−523.
4. Hall, D. H., and Hedgecock, E. M. (1991) Kinesin-related gene unc-104 is required for axonal transport of synaptic vesicles in *C. elegans*, *Cell 65*, 837−847.
5. Patel, N., Thierry-Mieg, D., and Mancillas, J. R. (1993) Cloning by insertional mutagenesis of a cDNA encoding *Caenorhabditis elegans* kinesin heavy chain, *Proc. Natl. Acad. Sci. U.S.A. 90*, 9181−9185.
6. Perkins, L. A., Hedgecock, E. M., Thomson, J. N., and Culotti, J. G. (1986) Mutant sensory cilia in the nematode *Caenorhabditis elegans*, *Dev. Biol. 117*, 456−487.
7. Wolf, F. W., Hung, M. S., Wightman, B., Way, J., and Garriga, G. (1998) Vab-8 is a key regulator of posteriorly directed migrations in *C. elegans* and encodes a novel protein with kinesin motor similarity, *Neuron 20*, 655−666.
8. Signor, D., Wedaman, K. P., Rose, L. S., and Scholey, J. M. (1999) Two heteromeric kinesin complexes in chemosensory neurons and sensory cilia of *Caenorhabditis elegans*, *Mol. Biol. Cell 10*, 345−360.
9. Raich, W. B., Moran, A. N., Rothman, J. H., and Hardin, J. (1998) Cytokinesis and midzone microtubule organization in *Caenorhabditis elegans* require the kinesin-like protein ZEN-4, *Mol. Biol. Cell 9*, 2037−2049.
10. Segbert, C., Barkus, R., Powers, J., Strome, S., Saxton, W. M., and Bossinger, O. (2003) KLP-18, a Klp2 kinesin, is required for assembly of acentrosomal meiotic spindles in *Caenorhabditis elegans*, *Mol. Biol. Cell 11*, 4458−4469.
11. Powers, J., Rose, D. J., Saunders, A., Dunkelbarger, S., Strome, S., and Saxton, W. M. (2004) Loss of KLP-19 polar ejection force causes misorientation and missegregation of holocentric chromosomes, *J. Cell Biol. 166*, 991−1001.
12. Mishima, M., Pavicic, V., Gruneberg, U., Nigg, E. A., and Glotzer, M. (2004) Cell cycle regulation of central spindle assembly, *Nature 430*, 908−913.
13. Lawrence, C. J., et al. (2004) A standardized kinesin nomenclature, *J. Cell Biol. 167*, 19−22.
14. Dagenbach, E. M., and Endow, S. A. (2004) A new kinesin tree, *J. Cell Sci. 117*, 3−7.
15. Combet, C., Blanchet, C., Geourjon, C., and Deléage, G. (2000) NPS@: Network Protein Sequence Analysis, *Trends Biol. Sci. 25*, 147−150.
16. Fraser, A. G., Kamath, R. S., Zipperlen, P., Martinez-Campos, M., Sohrmann, M., and Ahringer, J. (2000) Functional genomic analysis of *C. elegans* chromosome I by systematic RNA interference, *Nature 408*, 325−330.
17. Piano, F., Schetter, A. J., Mangone, M., Stein, L., and Kemphues, K. J. (2000) RNAi analysis of genes expressed in the ovary of *Caenorhabditis elegans*, *Curr. Biol. 10*, 1619−1622.
18. Dernburg, A. F., Zalevsky, J., Colaiacovo, M. P., and Villeneuve, A. M. (2000) Transgene-mediated cosuppression in the *C. elegans* germ line, *Genes Dev. 14*, 1578−1583.
19. Colaiacovo, M. P., Stanfield, G. M., Reddy, K. C., Reinke, V., Kim, S. K., and Villeneuve, A. M. (2002) A targeted RNAi screen for genes involved in chromosome morphogenesis and nuclear organization in the *Caenorhabditis elegans* germline, *Genetics 162*, 113−128.
20. Gunsalus, K. C., Yueh. W. C., MacMenamin, P., and Piano, F. (2004) RNAiDB and PhenoBlast: web tools for genome-wide phenotypic mapping projects, *Nucleic Acids Res. 1;32* Database issue: D406−D410.
21. Gill, S. C., and von Hippel, P. H. (1989) Calculation of protein extinction coefficients from amino acid sequence data, *Anal. Biochem. 182*, 319−326.
22. Gilbert, S. P., and Johnson, K. A. (1993) Expression, purification and characterisation of the *Drosophila* kinesin motor domain produced in *Escherichia coli*, *Biochemistry 32*, 4677−4684.
23. Bradford, M. M. (1976) A rapid and sensitive method for the quantitation of microgram quantities of protein utilizing the principle of protein-dye binding, *Anal. Biochem. 72*, 248−254.
24. Hackney, D. D., and Jiang, W. (2001) Assays for kinesin microtubule-stimulated ATPase activity, *Methods Mol. Biol. 164*, 65−71.
25. Schuck, P. (2000) Size-distribution analysis of macromolecules by sedimentation velocity ultracentrifugation and lamm equation modeling, *Biophys. J. 78*, 1606−1619.
26. Schuck, P. (1998) Sedimentation analysis of noninteracting and self-associating solutes using numerical solutions to the Lamm equation, *Biophys. J. 75*, 1503−1512.
27. Schuck, P., and Demeler, B. (1999) Direct sedimentation analysis of interference optical data in analytical ultracentrifugation, *Biophys. J. 76*, 2288−2296.
28. Foster, K. A., Correia, J. J., and Gilbert, S. P. (1998) Equilibrium binding studies of non-claret disjunctional protein (Ncd) reveal cooperative interactions between the motor domains, *J. Biol. Chem. 273*, 35307−35318.
29. Cochran, J. C., Sontag, C. A., Maliga, Z., Kapoor, T. M., Correia, J. J., and Gilbert, S. P. (2004) Mechanistic analysis of the mitotic kinesin Eg5, *J. Biol. Chem. 279*, 38861−38870.
30. Steinberg, G., and Schliwa, M. (1995) The *Neurospora* organelle motor: A distant relative of conventional kinesin with unconventional properties, *Mol. Biol. Cell 6*, 1605−1618.
31. Crevel, I., Carter, N., Schliwa, M., and Cross, R. (1999) Coupled chemical and mechanical reaction steps in a processive *Neurospora* kinesin, *EMBO J. 18*, 5863−5872.
32. Hyman, A. A. (1991) Preparation of marked microtubules for the assay of the polarity of microtubule-based motors by fluorescence, *J. Cell Sci. Suppl. 14*, 125−127.
33. Hyman, A., Drechsel, D., Kellogg, D., Salser, S., Sawin, K., Steffen, P., Wordeman, L., and Mitchison, T. (1991) Preparation of modified tubulins, *Methods Enzymol. 196*, 478−485.

34. Chandra, R., Salmon, E. D., Erickson, H. P., Lockhart, A., and Endow, S. A. (1993) Structural and functional domains of the *Drosophila* ncd microtubule motor protein, *J. Biol. Chem. 268*, 9005−9013.
35. Correia, J. J., Gilbert, S. P., Moyer, M. L., and Johnson, K. A. (1995) Sedimentation studies on the kinesin motor domain constructs K401, K366, and K341, *Biochemistry 34*, 4898−4907.
36. Huang, T. G., Suhan, J., and Hackney, D. D. (1994) *Drosophila* kinesin motor domain extending to amino acid position 392 is dimeric when expressed in *Escherichia coli*, *J. Biol. Chem. 269*, 16502−16507.
37. van Holde, K. E. (1975) *The Proteins*, Academic Press, New York.
38. Steinberg, G., and Schliwa, M. (1996) Characterization of the biophysical and motility properties of kinesin from the fungus *Neurospora crassa*, *J. Biol. Chem. 271*, 7516−7521.
39. Jiang, W., Stock, M., Li, X., and Hackney, D. D. (1997) Influence of the kinesin neck domain on dimerization and ATPase kinetics, *J. Biol. Chem. 272*, 7626−7632.
40. Tripet, B., Vale, S. D., and Hodges, R. S. (1997) Coiled-coil interactions within kinesin neck region using synthetic peptides, *J. Biol. Chem. 272*, 8946−8956.
41. Shimizu, T., Sablin, E., Vale, R. D., Fletterick, R., Pechatnikova, E., and Taylor, E. W. (1995) Expression, purification, ATPase properties, and microtubule-binding properties of the ncd motor domain, *Biochemistry 34*, 13259−13266.
42. Mackey, A. T., and Gilbert, S. P. (2003) The ATPase cross-bridge cycle of the Kar3 motor domain, *J. Biol. Chem. 278*, 3527−3535.
43. Kuriyama, R., Kofron, M., Essner, R., Kata, T., Dragos-Granoic, S., Omoto, C. K., and Khodjakov, A. (1995) Characterisation of a minus end-directed kinesin-like motor protein from cultured mammalian cells, *J. Cell Biol. 129*, 1049−1059.
44. Walker, R. A., Salmon, E. D., and Endow, S. A. (1990) The *Drosophila* claret segregregation protein is a minus-end directed motor molecule, *Nature 347*, 780−782.
45. deCastro, M. J., Ho, C.-H., and Stewart, R. J. (1999) Motility of dimeric ncd on a metal-chelating surfactant: Evidence that ncd is not processive, *Biochemistry 38*, 5076−5081.
46. Song, H., Golvkin, M., Reddy, A. S. N., and Endow, S. E. (1997) *In vitro* motility of AtKCBP, a calmodulin-binding kinesin protein of *Arabidopsis*, *Proc. Natl. Acad. Sci. U.S.A. 94*, 322−327.
47. Endow, S. A., Kang, S. J., Satterwhite, L. L., Rose, M. D., Skeen, V. P., and Salmon, E. D. (1994) Yeast Kar3 is a minus-end microtubule motor protein that destabilizes microtubules preferentially at the minus ends, *EMBO J. 13*, 2708−2713.
48. Matthies, H. J., McDonald, H. B., Goldstein, L. S., and Theurkauf, W. E. (1996) Anastral meiotic spindle morphogenesis: role of the non-claret disjunctional kinesin-like protein, *J. Cell Biol. 134*, 455−464.
49. Hirel, P. H., Schmitter, M. J., Dessen, P., Fayat, G., and Blanquet, S. (1989) Extent of N-terminal methionine excision from *Escherichia coli* proteins is governed by the side-chain length of the penultimate amino acid, *Proc. Natl. Acad. Sci. U.S.A. 85*, 8247−8251.
50. Lupas, A., Van Dyke, M., and Stock, J. (1991) Predicting coiled-coils from protein sequences, *Science 252*, 1162−1164.
51. Berger, B., Wilson, D. B., Wolf, E., Tonchev, T., Milla, M., and Kim, P. S. (1995) Predicting Coiled Coils by Use of Pairwise Residue Correlations, *Proc. Natl. Acad. Sci. U.S.A. 92*, 8259−8263.

BI048157H